

Influence of microwave fields on the electron transport through a quantum dot in the presence of a direct tunneling between leads

R. Taranko¹, T. Kwapiński, E. Taranko

Institute of Physics, M. Curie-Skłodowska University,
20-031 Lublin, Poland

Abstract

We consider the time-dependent electron transport through a quantum dot coupled to two leads in the presence of the additional over-dot (bridge) tunneling channel. By using the evolution operator method together with the wide-band limit approximation we derived the analytical formulae for the quantum dot charge and current flowing in the system. The influence of the external microwave field on the time-average quantum dot charge, the current and the derivatives of the average current with respect to the gate and source-drain voltages has been investigated for a wide range of parameters.

1 Introduction

Electronic transport in mesoscopic systems has been at the focus of experimental and theoretical interest during the last decade due to recent development in fabrication of small electronic devices and their interesting equilibrium and non-equilibrium properties. Especially interesting are the transport properties of a quantum dot (QD) under the influence of external time-dependent fields. The high-frequency signals may be applied to a QD and the time-dependent fields will modify the tunneling current.

New effects have been observed and theoretically described, e.g. photon-assisted tunneling through small quantum dots with well-resolved discrete energy states [1, 2, 3], photon-electron pumps [4, 5, 6] and others. One can investigate the current flowing

¹corresponding author, e-mail: taranko@tytan.umcs.lublin.pl

through a QD under periodic modulation of the QD electronic structure [7] or periodic (non-periodic) modulation of the tunneling barriers [6] and electron energy levels in both (left and right) electron reservoirs [8] (see also [9, 10]).

The progress of nanomaterials science has enabled the experimental study of the phase coherence of the charge carriers in many mesoscopic systems. The asymmetric Fano line shapes [11] are observed whenever resonant and nonresonant scattering paths interfere. In some nanostructures, e.g. in single-electron transistors, the Fano resonances in the conductance were observed [12], which imply that there are two paths for transfer of electrons between a source and a drain. Especially the recent experimental and theoretical study with a low-temperature scanning tunneling microscope (STM) of the single magnetic atom deposited on a metallic surface showed the asymmetric Fano resonances in the tunneling spectra [12–15]. The STM measurements indicate that in tunneling of electrons between STM tip and a surface with a single impurity atom two different paths are present. The electrons can tunnel between the tip and the adsorbate state and directly between the tip and the metal surface. The electronic transport through a QD coupled to the electron reservoirs within a model with two electron tunneling channels was considered in Ref. [16] and it was shown, that transport of electrons through both channels leads to an asymmetric shape of the zero bias voltage conductance curves, which is typical behaviour for a Fano resonance resulting from constructive and destructive interference processes for electrons transmitted through both channels.

In all papers mentioned above and relating to the electron transport through a QD with the additional (bridge) transmission channel the external fields were not applied and the considered systems were driven out of equilibrium only by means of a dc voltage bias. In this paper we address the issue of a QD with a bridge channel between a source and a drain driven out of equilibrium by means of a dc voltage bias and additional time-dependent external fields. In this manner, our paper can be seen as generalization of Ref. [9] to the case of a QD with the additional bridge channel in the presence of external microwave fields which are applied to the dot and two leads, respectively. In literature, different theoretical approaches have been developed to treat the time-dependent, nonequilibrium electron transport processes in the mesoscopic systems. It seems, that the most popular is the nonequilibrium Green's function method. However, these Green's functions depend on the time arguments and for non trivial quantum models it is a rather difficult task to calculate them. In our treatment of the time-dependent tunneling through

a mesoscopic system we use the evolution operator technique (e.g. [17, 18]). The final expressions for the QD charge and the current flowing in the system can be described in terms of the corresponding matrix elements of the evolution operator. In our earlier work [19] we have considered the similar problem solving numerically the corresponding sets of the differential equations satisfied by the matrix elements of the evolution operator. Due to the complexity and a large number of these equations we considered only a very limited number of interesting cases although we were able to take into consideration the electronic structure of the lead energy bands and the specific time-dependence of the QD-lead barriers. Here we give the analytical expressions for the QD charge and current assuming so called the wide-band limit approximation and the time-independent strength of the QD-lead barriers. As a result, due to these analytical forms, we are able to analyze the required characteristics of the considered system for the very broad class of parameters. Additionally, due to the final forms given for some matrix elements of the evolution operator it is possible to build up the expressions for the QD charge or current in the form of the perturbation series.

In the next Section we present the model and formalism and give the resulting expressions for equations for the corresponding matrix elements of the evolution operator. In Section 3 we obtain the approximate solutions for all required matrix elements and give the final forms for the QD charge and the current flowing in the system. The results are presented in Section 4 which includes also the summary and a brief discussion.

2 Model and calculation method

We model the QD coupled to the left and right electron reservoirs with the additional bridge tunneling channel between them by the usually used Hamiltonian $H = H_1 + V$, where

$$H_1 = \sum_{\vec{k}_\alpha} \varepsilon_{\vec{k}_\alpha}(t) a_{\vec{k}_\alpha}^+ a_{\vec{k}_\alpha} + \varepsilon_d(t) a_d^+ a_d, \quad (1)$$

$$V = \sum_{\vec{k}_\alpha} V_{\vec{k}_\alpha d}(t) a_{\vec{k}_\alpha}^+ a_d + \text{h.c.} + \sum_{\vec{k}_L, \vec{k}_R} V_{\vec{k}_L \vec{k}_R}(t) a_{\vec{k}_L}^+ a_{\vec{k}_R} + \text{h.c.} \quad (2)$$

The operators $a_{\vec{k}_\alpha}^-$ ($a_{\vec{k}_\alpha}^+$), a_d (a_d^+) are the annihilation (creation) operators of the electron in the lead α ($\alpha = L, R$) and in the QD, respectively. The couplings between QD and lead states and between both lead states are denoted by $V_{\vec{k}_\alpha d}$ and $V_{\vec{k}_L \vec{k}_R}$, respectively. For

simplicity, the dot is characterized only by a single level ε_d and we have neglected the intradot electron-electron Coulomb interaction. We assume the case in which there exist microwave fields applied to the leads and QD. In the adiabatic approximation our time-dependent driven system is described by $\varepsilon_{\vec{k}_\alpha}(t) = \varepsilon_{\vec{k}_\alpha} + \Delta_\alpha \cos \omega t$, $\varepsilon_d(t) = \varepsilon_d + \Delta_d \cos \omega t$, i.e. the energy levels of the leads and QD are driven by the ac field with the frequency ω and the amplitudes Δ_α and Δ_d , respectively.

We describe the dynamical evolution of the charge localised on the QD and the current flowing in the system in terms of the time evolution operator $U(t, t_0)$ (in the interaction representation) which satisfies the equation

$$i \frac{\partial}{\partial t} U(t, t_0) = \tilde{V}(t) U(t, t_0), \quad (3)$$

where

$$\tilde{V}(t) = U_0(t, t_0) V(t) U_0^\dagger(t, t_0), \quad (4)$$

$$U_0(t) = T \exp \left(i \int_{t_0}^t dt' H_1(t') \right). \quad (5)$$

Here we assume that the interaction between QD and leads and between both leads is switched on in the distant past t_0 , i.e. $V_{\vec{k}_\alpha d}(t)$ and $V_{\vec{k}_L \vec{k}_R}(t)$ equal to zero for $t \leq t_0$ and takes constant values for $t > t_0$.

The QD charge and currents flowing in the system can be obtained from the knowledge of the appropriate matrix elements of the evolution operator $U(t, t_0)$. The QD charge is given as follows (cf. [18]):

$$n_d(t) = n_d(t_0) |U_{dd}(t, t_0)|^2 + \sum_{\vec{k}_\alpha} n_{\vec{k}_\alpha}(t_0) |U_{d\vec{k}_\alpha}(t, t_0)|^2, \quad (6)$$

where $U_{dd}(t, t_0) \equiv \langle d | U(t, t_0) | d \rangle$ and $U_{d\vec{k}_\alpha}(t, t_0) \equiv \langle d | U(t, t_0) | \vec{k}_\alpha \rangle$ denote the matrix elements of $U(t, t_0)$ calculated within the basis functions containing the electron single-particle functions of the leads and QD, $|\vec{k}_L\rangle$, $|\vec{k}_R\rangle$ and $|d\rangle$, respectively. $n_d(t_0)$ and $n_{\vec{k}_\alpha}(t_0)$ represent the initial filling of the corresponding single-particle states.

The tunneling current flowing, e.g. from the left lead into the QD and the right lead, $j_L(t)$, can be obtained from the time derivative of the total number of electrons in the left lead, $j_L(t) = -e dn_L(t)/dt$ (cf. [9]), where

$$\begin{aligned} n_L(t) &= \sum_{\vec{k}_L} n_{\vec{k}_L}(t) = \sum_{\vec{k}_L} (n_d(t_0) |U_{\vec{k}_L d}(t, t_0)|^2 \\ &+ \sum_{\vec{q}_L} n_{\vec{q}_L}(t_0) |U_{\vec{k}_L, \vec{q}_L}(t, t_0)|^2 + \sum_{\vec{k}_R} n_{\vec{k}_R}(t_0) |U_{\vec{k}_L, \vec{k}_R}(t, t_0)|^2). \end{aligned} \quad (7)$$

Let us begin with the calculations of the QD charge $n_d(t)$. Then we have to calculate the matrix elements $U_{dd}(t, t_0)$ and $U_{d\vec{k}_\alpha}(t, t_0)$. Using the identity operator $I = |d\rangle\langle d| + \sum_{\vec{k}_\alpha} |\vec{k}_\alpha\rangle\langle\vec{k}_\alpha|$ the following set of coupled equations can be obtained from Eq. (3):

$$\frac{\partial}{\partial t} U_{dd}(t, t_0) = -i \sum_{\vec{k}_{\alpha d}} \tilde{V}_{\vec{k}_{\alpha d}}^*(t) U_{\vec{k}_{\alpha d}}(t, t_0), \quad (8)$$

$$\frac{\partial}{\partial t} U_{\vec{k}_L d}(t, t_0) = -i \tilde{V}_{\vec{k}_L d}(t) U_{dd}(t, t_0) - i \sum_{\vec{k}_R} \tilde{V}_{\vec{k}_L \vec{k}_R}(t) U_{\vec{k}_R d}(t, t_0), \quad (9)$$

$$\frac{\partial}{\partial t} U_{\vec{k}_R d}(t, t_0) = -i \tilde{V}_{\vec{k}_R d}(t) U_{dd}(t, t_0) - i \sum_{\vec{k}_L} \tilde{V}_{\vec{k}_R \vec{k}_L}(t) U_{\vec{k}_L d}(t, t_0), \quad (10)$$

where

$$\begin{aligned} \tilde{V}_{\vec{k}_{\alpha d}}(t) &\equiv \langle \vec{k}_\alpha | \tilde{V}(t) | d \rangle = V_{\vec{k}_{\alpha d}} \exp(i(\varepsilon_\alpha - \varepsilon_d)(t - t_0)) \\ &\quad - i(\Delta_d - \Delta_\alpha)(\sin \omega t - \sin \omega t_0)/\omega, \end{aligned} \quad (11)$$

$$\begin{aligned} \tilde{V}_{\vec{k}_L \vec{k}_R}(t) &\equiv \langle \vec{k}_L | \tilde{V}(t) | \vec{k}_R \rangle = V_{\vec{k}_L \vec{k}_R} \exp(i(\varepsilon_{\vec{k}_L} - \varepsilon_{\vec{k}_R})(t - t_0) - \\ &\quad - i(\Delta_L - \Delta_R)(\sin \omega t - \sin \omega t_0)/\omega). \end{aligned} \quad (12)$$

It is easy to show that the equation for $U_{dd}(t, t_0)$ can be written as follows:

$$\frac{\partial U_{dd}(t, t_0)}{\partial t} = - \int_{t_0}^t dt' (\mathcal{K}(t, t') U_{dd}(t', t_0) + \sum_{\vec{k}_\alpha} \mathcal{L}_{\vec{k}_\alpha}(t, t') U_{\vec{k}_\alpha d}(t', t_0)), \quad (13)$$

where

$$\mathcal{K}(t, t') = \sum_{\vec{k}_\alpha} \tilde{V}_{\vec{k}_{\alpha d}}^*(t) \tilde{V}_{\vec{k}_{\alpha d}}(t'), \quad (14)$$

$$\mathcal{L}_{\vec{k}_L}(t, t') = \sum_{\vec{k}_R} \tilde{V}_{\vec{k}_R}^*(t) \tilde{V}_{\vec{k}_R \vec{k}_L}(t'), \quad (15)$$

and the similar equation can be written for $\mathcal{L}_{\vec{k}_R}(t, t')$.

The formal solution of Eq. (9) written in the form

$$U_{\vec{k}_L d}(t, t_0) = -i \int_{t_0}^t dt' \tilde{V}_{\vec{k}_L d}(t') U_{dd}(t', t_0) - i \sum_{\vec{k}_R} \int_{t_0}^t dt' \tilde{V}_{\vec{k}_L \vec{k}_R}(t') U_{\vec{k}_R d}(t'), \quad (16)$$

(and the similar equation for $U_{\vec{k}_R d}(t, t_0)$) can be iterated giving

$$\begin{aligned} U_{Ld}(t, t_0) &= -i \int_{t_0}^t dt_1 \tilde{V}_L(t_1) U_{dd}(t_1, t_0) \\ &+ \sum_{j=2}^{\infty} (-i)^j \sum_{R_1, L_2, R_3, L_4, \dots, \alpha_{j-1}} \int_{t_0}^t dt_1 \dots \int_{t_0}^{t_{j-1}} dt_j \tilde{V}_{L R_1}(t_1) \tilde{V}_{R_1 L_2}(t_2) \dots \tilde{V}_{\alpha_{j-1}}(t_j) \cdot U_{dd}(t_j, t_0). \end{aligned} \quad (17)$$

Here we have introduced the abbreviated form for the vector \vec{k}_α and replaced it by α and $\tilde{V}_{\vec{k}_\alpha d}(t) \equiv \tilde{V}_\alpha(t)$. The equation for $U_{Rd}(t, t_0)$ can be obtained from Eq. (17) by interchanging $L \leftrightarrow R$. Inserting these expressions for $U_{Ld}(t, t_0)$ and $U_{Rd}(t, t_0)$ into Eq. (13) one obtains the closed integro-differential equation for $U_{dd}(t, t_0)$

$$\begin{aligned} \frac{\partial}{\partial t} U_{dd}(t, t_0) &= - \int_{t_0}^t dt_1 \mathcal{K}(t, t_1) U_{dd}(t_1, t_0) \\ &- \sum_{j=2}^{\infty} (-i)^{j-1} \sum_{L_1, R_2, L_3, \dots, \alpha_j} \int_{t_0}^t dt_1 \dots \int_{t_0}^{t_{j-1}} dt_j \tilde{V}_{L_1}^*(t) \tilde{V}_{L_1 R_2}(t_1) \dots \tilde{V}_{\alpha_j}(t_j) U_{dd}(t_j, t_0) \\ &+ (\text{the second term with the change } L \leftrightarrow R). \end{aligned} \quad (18)$$

Equation (18) together with the expressions for $\tilde{V}_L(t)$ and $\tilde{V}_{LR}(t)$, Eqs. (11, 12), and for $\mathcal{K}(t, t_1)$ written as follows

$$\mathcal{K}(t, t_1) = \sum_{\alpha=L,R} |V_\alpha|^2 \mathcal{D}_\alpha(t - t_1) \exp(i\varepsilon_d(t - t_1) + i(\Delta_d - \Delta_\alpha)(\sin \omega t - \sin \omega t_1)/\omega) \quad (19)$$

where $\mathcal{D}_\alpha(t)$ a Fourier transform of the α -th lead density of states, gives exact, closed equation for $U_{dd}(t, t_0)$. Here we have assumed that $V_{\vec{k}_\alpha}$ does not depend on the wave vector \vec{k}_α and then the similar assumption will be made for $V_{\vec{k}_L \vec{k}_R}$.

Under the wide-band limit (WBL) approximation (e.g. [9]) this equation can be analytically solved and such solutions will be considered later. Formally, solving Eq. (18) and inserting its solution to Eq. (17), the solutions for $U_{Ld}(t, t_0)$ and $U_{Rd}(t, t_0)$ can be obtained. These functions are needed in the calculations of the first term of $j_L(t)$ (see Eq. 7).

In order to calculate $n_d(t)$ we still need $U_{d\alpha}(t, t_0)$. Writing down the set of closed equations for $U_{dR}(t, t_0)$, $U_{R_1 R_2}(t, t_0)$ and $U_{LR}(t, t_0)$ (obtained on the basis of Eq. (3)) and performing similar calculations to those described above, one obtains for $U_{dR}(t, t_0)$ (and similar equation for $U_{dL}(t, t_0)$ by interchanging $L \leftrightarrow R$):

$$\begin{aligned} \frac{\partial}{\partial t} U_{dR}(t, t_0) &= \\ &- i\tilde{V}_R^*(t) + (-i)^2 \int_{t_0}^t dt_1 \sum_L \tilde{V}_L^*(t) \tilde{V}_{LR}(t_1) \\ &+ \sum_{j=2,4,6,\dots}^{\infty} (-i)^{j+1} \sum_{R_1, L_2, R_3, \dots, L_j} \int_{t_0}^t dt_1 \dots \int_{t_0}^{t_{j-1}} dt_j \tilde{V}_{R_1}^*(t) \tilde{V}_{R_1 L_2}(t_1) \dots \tilde{V}_{L_j R}(t_j) \\ &+ \sum_{j=3,5,7,\dots}^{\infty} (-i)^{j+1} \sum_{L_1, R_2, L_3, \dots, L_j} \int_{t_0}^t dt_1 \dots \int_{t_0}^{t_{j-1}} dt_j \tilde{V}_{L_1}^*(t) \tilde{V}_{L_1 R_2}(t_1) \dots \tilde{V}_{L_j R}(t_j) \end{aligned}$$

$$\begin{aligned}
& + (-i)^2 \int_{t_0}^t dt_1 \sum_L \tilde{V}_L^*(t) V_L(t_1) U_{dR}(t_1, t_0) \\
& + \sum_{j=2}^{\infty} (-i)^{j+1} \sum_{L_1, R_2, L_3, \dots, \alpha_j} \int_{t_0}^t dt_1 \dots \int_{t_0}^{t_{j-1}} dt_j \tilde{V}_{L_1}^*(t) \tilde{V}_{L_1 R_2}(t_1) \dots \tilde{V}_{\alpha_j}(t_j) U_{dR}(t_j, t_0), \quad (20)
\end{aligned}$$

and for $U_{LR}(t, t_0)$ (needed for calculation of the last term of $n_L(t)$, Eq. (7)):

$$\begin{aligned}
U_{LR}(t, t_0) & = -i \int_{t_0}^t dt_1 \tilde{V}_{LR}(t_1) \\
& + \sum_{j=3,5,7\dots}^{\infty} (-i)^j \sum_{R_1, L_2, R_3, \dots, L_{j-1}} \int_{t_0}^t dt_1 \int_{t_0}^{t_1} dt_2 \dots \int_{t_0}^{t_{j-1}} dt_j \tilde{V}_{LR}(t_1) \tilde{V}_{R_1 L_2}(t_2) \dots \tilde{V}_{L_{j-1} R}(t_j) \\
& - i \int_{t_0}^t dt_1 \tilde{V}_L(t_1) U_{dR}(t_1, t_0) \quad (21) \\
& + \sum_{j=2}^{\infty} (-i)^j \sum_{R_1, L_2, \dots, \alpha_{j-1}} \int_{t_0}^t dt_1 \int_{t_0}^{t_1} dt_2 \dots \int_{t_0}^{t_{j-1}} dt_j \tilde{V}_{LR_1}(t_1) \tilde{V}_{R_1 L_2}(t_2) \dots \tilde{V}_{\alpha_j}(t_j) U_{dR}(t_j, t_0).
\end{aligned}$$

The analytical solutions of these equations under the WBL approximation will be discussed in the next section.

For calculation of $n_{\bar{k}_L}(t)$ one needs the functions $U_{Ld}(t, t_0)$, $U_{LR}(t, t_0)$ and $U_{L_1 L_2}(t, t_0)$. The first two functions are given in Eqs. (17) and (21) and $U_{L_1 L_2}(t, t_0)$ should be calculated from the set of coupled equations for $U_{dL}(t, t_0)$, $U_{L_1 L_2}(t, t_0)$ and $U_{RL}(t, t_0)$ obtained from Eq. (3). The result is as follows:

$$\begin{aligned}
U_{L_1 L}(t, t_0) & = \delta_{L_1 L} + \sum_{j=2,4,\dots}^{\infty} (-i)^j \sum_{R_1, L_2, R_3, \dots, R_{j-1}} \int_{t_0}^t dt_1 \int_{t_0}^{t_1} dt_2 \dots \int_{t_0}^{t_{j-1}} dt_j \tilde{V}_{L_1 R_1}(t_1) \tilde{V}_{R_1 L_2}(t_2) \dots \tilde{V}_{R_{j-1} L}(t_j) \\
& - i \int_{t_0}^t dt_1 \tilde{V}_{L_1}^*(t_1) U_{dL}(t_1, t_0) \quad (22) \\
& + \sum_{j=2}^{\infty} (-i)^j \sum_{R_1, L_2, R_3, \dots, \alpha_{j-1}} \int_{t_0}^t dt_1 \int_{t_0}^{t_1} dt_2 \dots \int_{t_0}^{t_{j-1}} dt_j \tilde{V}_{L_1 R_1}(t_1) \tilde{V}_{R_1 L_2}(t_2) \dots \tilde{V}_{\alpha_{j-1} L}(t_j) U_{dL}(t_j, t_0),
\end{aligned}$$

where $U_{dL}(t, t_0)$ is given by solving Eq. (20) with the replacement $L \leftrightarrow R$.

3 Analytical solutions in the WBL approximation

In order to calculate the QD charge $n_d(t)$ or current $j_L(t)$ one has to solve, in the first step, the integro-differential equations satisfied by $U_{dd}(t, t_0)$, Eq. (18), and $U_{dR/L}(t, t_0)$, Eq. (20). The other needed functions $U_{Ld}(t, t_0)$, $U_{L_1 L_2}(t, t_0)$ and $U_{LR}(t, t_0)$ can be obtained from Eqs. (17, 21, 22) inserting into them $U_{dd}(t, t_0)$, $U_{dL/R}(t, t_0)$ and performing

multiple time and \vec{k} -vector integrations. Unfortunately, it is a very difficult task to solve the integro-differential equations and to perform these integrals in a general case when the leads are characterized by some density of state curves. Here, we use the WBL approximation, under which all multiple time and \vec{k} -vectors integrals can be performed without difficulties. The WBL approximation has been widely used in calculating of many properties of mesoscopic systems (e.g. [2, 3, 5, 9, 10]). It is justified under the conditions that the QD energy level linewidth is much smaller than the bandwidth of the leads and that the density of states and hopping matrix elements vary slowly with energy. Furthermore, as we are not going to consider the case of the QD energy level lying close to the edges of the leads energy band or lying close to some singular structure present in the leads density of states, then application of the WBL approximation should be fully justified. The conditions under which we perform our calculations are satisfied in most experimental constructions of mezosopic systems. As a check, we have performed the direct but time consuming numerical integration of Eqs. (8–10) (and similar equations for other functions) for the rectangular leads density of states and did not find any differences in the results for the time-averaged QD charge or the currents flowing in the considered system. Therefore, in this section we consider the electron transport through the QD with the additional bridge tunnel over the dot within the WBL approximation. In this approach the solutions of the integro-differential Eqs. (19) and (20) in the analytical form can be obtained and the infinite sums of all terms in Eqs. (17) and (21) can be calculated.

Let us consider the equation for the matrix element $U_{dd}(t, t_0)$, Eq. (18). The function $\mathcal{K}(t, t')$, Eq. (19), is approximated in WBL as follows

$$\begin{aligned} \mathcal{K}(t, t_1) &= \sum_{\alpha} |V_{\alpha}|^2 \int_{-\infty}^{\infty} d\varepsilon \mathcal{D}_{\alpha}(\varepsilon) \exp(-i\varepsilon(t - t_1)) \exp(-i\varepsilon_d(t - t_1)) \\ &\quad + i(\Delta_d - \Delta_{\alpha})(\sin \omega t - \sin \omega t_1)/\omega \Rightarrow \\ &\Rightarrow \sum_{\alpha} \frac{|V_{\alpha}|^2}{D_{\alpha}} 2\pi \delta(t - t_1), \end{aligned} \quad (23)$$

where the leads density of states $\mathcal{D}_{\alpha}(\varepsilon)$ was replaced by the rectangular density of states with the "effective" bandwidth D_{α}

Using similar approximation in calculations of the multiple integrals present in Eq. (18) one obtains

$$\frac{\partial}{\partial t} U_{dd}(t, t_0) = \left(-\frac{\Gamma}{2} - \frac{2V^2\pi}{D} \sum_{j=1}^{\infty} (-i\pi V_{RL}/D)^j \right) U_{dd}(t, t_0), \quad (24)$$

where $\Gamma_{\alpha} = 2\pi V^2/D$, $\Gamma = \Gamma_L + \Gamma_R$, $D_L = D_R = D$, $V \equiv V_{\alpha}$.

Assuming $\pi V_{RL}/D < 1$ the series can be summed up and finally the equation for $U_{dd}(t, t_0)$ reads

$$\frac{\partial}{\partial t} U_{dd}(t, t_0) = -C_1 U_{dd}(t, t_0), \quad (25)$$

where $C_1 = (2\pi V^2/D)/(1 + i\pi V_{RL}/D)$.

Similarly, Eq. (20) becomes

$$\frac{\partial}{\partial t} U_{d\alpha}(t, t_0) = -i\tilde{V}_{dd}(t)/(1 + iV_{RL}\pi/D) - C_1 U_{d\alpha}(t, t_0). \quad (26)$$

The solutions of Eqs. (25) and (26) are as follows:

$$U_{dd}(t, t_0) = \exp(-C_1(t - t_0)), \quad (27)$$

$$U_{d\alpha}(t, t_0) = -i/(1 + iV_{RL}\pi/D) \int_{t_0}^t dt_1 \tilde{V}_{d\alpha}(t_1) \exp(-C_1(t - t_1)) \quad (28)$$

and the QD charge $n_d(t)$ can be easily obtained, Eq. (6). It can be verified, that the first term of Eq. (6) tends to zero as $t - t_0 \rightarrow \infty$ and finally for the QD charge we have

$$n_d(t) = \frac{1}{(1 + (V_{RL}\pi/D)^2)} \sum_{\alpha} \frac{\Gamma_{\alpha}}{2\pi} \int d\varepsilon f_{\alpha}(\varepsilon) |A_{\alpha}(\varepsilon, t)|^2, \quad (29)$$

where

$$A_{\alpha}(\varepsilon, t) = - \int_{t_0}^t dt_1 \exp(i(\varepsilon_d - \varepsilon)(t - t_1) - i(\Delta_d - \Delta_{\alpha})(\sin \omega t - \sin \omega t_1)/\omega - C_1(t - t_1)) \quad (30)$$

In the limit of vanishing bridge over the QD, Eq. (29) reproduces the result of Ref. [9].

The current $j_L(t)$ flowing from the left lead into the QD and the right lead is calculated from the evolution of the total number of electrons in the left lead (see Eq. 7) and one can read:

$$\begin{aligned} j_L(t) = & 2\text{Re} \left\{ n_d(t_0) \sum_{\vec{k}_L} U_{\vec{k}_L d}^*(t, t_0) \frac{d}{dt} U_{\vec{k}_L d}(t, t_0) \right. \\ & + \sum_{\vec{k}_L, \vec{q}_L} n_{\vec{q}_L}(t_0) U_{\vec{k}_L, \vec{q}_L}^*(t, t_0) \frac{d}{dt} U_{\vec{k}_L, \vec{q}_L}(t, t_0) \\ & \left. + \sum_{\vec{k}_L, \vec{k}_R} n_{\vec{k}_R}(t_0) U_{\vec{k}_L, \vec{k}_R}^*(t, t_0) \frac{d}{dt} U_{\vec{k}_L, \vec{k}_R}(t, t_0) \right\}. \quad (31) \end{aligned}$$

The functions $U_{\vec{k}_L d}$, $U_{\vec{k}_L, \vec{q}_L}$ and $U_{\vec{k}_L, \vec{k}_R}(t, t_0)$ are calculated according to Eqs. (17), (22) and (21), respectively, and after summing up of the corresponding multiple integrals one

obtains:

$$U_{\vec{k}_L d}(t, t_0) = -\frac{i}{1+ix} \int_{t_0}^t dt_1 \tilde{V}_{\vec{k}_L d}(t_1) U_{dd}(t_1, t_0), \quad (32)$$

$$\begin{aligned} U_{\vec{k}_L, \vec{q}_L}(t, t_0) &= \delta_{\vec{k}_L, \vec{q}_L} - \frac{V_{RL} \cdot x}{1+x^2} \int_{t_0}^t dt_1 \exp\{i(\varepsilon_{\vec{k}_L} - \varepsilon_{\vec{q}_L})(t_1 - t_0)\} \\ &\quad - \frac{i}{1+ix} \int_{t_0}^t dt_1 \tilde{V}_{\vec{k}_L d}(t_1) U_{d\vec{q}_L}(t_1, t_0), \end{aligned} \quad (33)$$

$$\begin{aligned} U_{\vec{k}_L, \vec{k}_R}(t, t_0) &= -\frac{i}{1+ix} \int_{t_0}^t dt_1 \tilde{V}_{\vec{k}_L d}(t_1) U_{d\vec{k}_R}(t_1, t_0) \\ &\quad - \frac{i}{1+x^2} \int_{t_0}^t dt_1 \tilde{V}_{\vec{k}_L \vec{k}_R}(t_1), \end{aligned} \quad (34)$$

where $U_{dd}(t, t_0)$, $U_{d\vec{k}_L}(t, t_0)$ and $U_{d\vec{k}_R}(t, t_0)$ are given in Eqs. (27, 28) and $x = \pi V_{RL}/D$. One can verify, that the first term in Eq. (31) tends to zero for $t - t_0 \rightarrow \infty$ as we have for this term

$$n_d(t_0) |1/(1+ix)|^2 \Gamma/2 \exp(-\Gamma(t-t_0) ReC_2), \quad (35)$$

where $ReC_2 = Re(1/(1+ix)) > 0$.

The second and third terms of the expression for $j_L(t)$, Eq. (30), together with Eqs. (27, 28, 31-33) give finally the time averaged current:

$$\begin{aligned} \langle j_L(t) \rangle &= \frac{1}{\pi} \frac{2x^2}{(1+x^2)^2} \int (f_R(\varepsilon) - f_L(\varepsilon)) d\varepsilon + \frac{\Gamma/2}{1+x^2} \langle n_d(t) \rangle \\ &\quad + \text{Im} \left\{ \frac{1-x^2}{(1+x^2)(1+ix)^2} \frac{\Gamma_L}{\pi} \int d\varepsilon f_L(\varepsilon) \langle A_L(\varepsilon, t) \rangle \right\} \\ &\quad + \text{Re} \left\{ \frac{2x}{(1+x^2)(1+ix)} \frac{\Gamma_L}{\pi} \int d\varepsilon f_R(\varepsilon) \langle A_R(\varepsilon, t) \rangle \right\}. \end{aligned} \quad (36)$$

In the vanishing bridge channel case Eq. (35) coincides with the results of Ref. [9]:

$$\langle j_L^{V_{RL}=0}(t) \rangle = \frac{\Gamma}{2} \langle n_d(t) \rangle + \frac{\Gamma_L}{\pi} \int d\varepsilon f_L(\varepsilon) \text{Im} \langle A_L(\varepsilon, t) \rangle. \quad (37)$$

The current $\langle j_L(t) \rangle$, Eq. (36), flowing from the left lead to the central region and to the right lead (through the bridge channel) is the superposition of four terms. The first term corresponds to the current between two leads and this term is not disturbed by the QD. The form of the second and third terms is the same as for $\langle j_L^{V_{RL}=0}(t) \rangle$, Eq. (37), except for the renormalization constants due to the additional tunneling channel. Note, that some additional renormalizations also occur due to V_{RL} which enters into the expression for $n_d(t)$, Eq. (29), and for $A_\alpha(\varepsilon, t)$, Eq. (30). The last term of Eq. (36) is the interference term due to the simultaneous tunneling through two channels.

4 Results and discussion

Here we show the numerical results of the time-averaged QD charge $\langle n_d(t) \rangle$ and the current $\langle j_L(t) \rangle$ and its derivatives with respect to the QD energy level position and the chemical potential μ_L (or equivalently, with respect to the gate and source-drain voltages) for different sets of parameters which characterize our system. We assume the temperature $T = 0$ K and the time-average of time-dependent quantities $f(t)$ is defined by

$$\langle f(t) \rangle = \lim_{2\tau \rightarrow \infty} \frac{1}{2\tau} \int_{-\tau}^{\tau} dt' f(t'), \quad (38)$$

and because $f(t)$ is a periodic function of time, we average it over the period $2\pi/\omega$. We take the chemical potential of the right lead μ_R as the energy measurement point, $\mu_R = 0$. As the potential drop between the left and right leads is given by $\mu_L - \mu_R = eV_{s-d}$ and V_{s-d} is the measured voltage between a source and a drain, then the derivatives of the current $\langle j_L(t) \rangle$ with respect to μ_L will correspond to the derivatives $d\langle j_L(t) \rangle / dV_{s-d}$ usually measured in experiments. In experiments the gate voltage controls the position of the QD energy level ε_d (regardless how complicated the relation between the gate voltage and ε_d is) and for that reason to mimic measurements of the QD charge or current vs. the gate voltage we have calculated them vs. the position of the QD energy level ε_d .

The values of the hybridization matrix elements $V_{\vec{k}_{\alpha}d}$ present in the Hamiltonian do not enter the final expressions for the current or QD charge obtained within the WBL approximation. Usually the effective linewidth $\Gamma_{\alpha} = 2\pi \sum_{\vec{k}_{\alpha}} |V_{\vec{k}_{\alpha}d}|^2 \delta(E - \varepsilon_{\vec{k}_{\alpha}})$ is introduced. However, in our calculations the others hybridization matrix elements appear, $V_{\vec{k}_R, \vec{k}_L} \equiv V_{RL}$, responsible for the additional tunneling channel for which we should take some values in order to perform numerical calculations. We have taken the values comparable with $V_{\vec{k}_{\alpha}d}$ and estimated $V_{\vec{k}_{\alpha}d}$ (assuming its \vec{k} -independence, $V_{\vec{k}_{\alpha}d} \equiv V_{\alpha} = V$) using the relation $\Gamma_{\alpha} = 2\pi |V_{\alpha}|^2 / D_{\alpha}$, where D_{α} is the α -lead's bandwidth and $D_{\alpha} = 100 \Gamma_{\alpha}$ ($\Gamma_L = \Gamma_R = \Gamma$, $D_L = D_R = D$ was assumed). We assumed the amplitude of the QD energy levels oscillation Δ_d to be one half of Δ_L and $\Delta_R = 0$, if otherwise stated. In our calculations the values V_{RL} were taken from the range (0–10), in Γ units.

In the first three figures, Figs. 1–3, we present the overall shape of the average current $\langle j_L(t) \rangle$ and the derivatives of the average current with respect to the QD energy level ε_d and the left chemical potential μ_L , respectively, against ε_d and μ_L . The upper panels correspond to the $V_{RL} = 0$ case and the lower ones present the results obtained for

the non-vanishing over-dot tunneling channel, $V_{RL} \neq 0$. There are quite visible differences between the case of a QD with and without additional bridge tunneling channel (cf. upper and lower panels in Figs 1–3). For better visualization of the peculiarities of the presented functions and for simpler discussion let us consider the specific cuts of the surfaces given in Figs. 1-3.

At first, let us consider the dependence of $\langle j_L(t) \rangle$ vs. ε_d for given values of the left lead chemical potential μ_L . In Fig. 4 we present such curves for different values of μ_L – the subsequent curves beginning from the lower one correspond to $\mu_L = -4$ up to the upper curve (with the step $\Delta\mu_L = 1$) obtained for $\mu_L = 8$. The left (right) panel corresponds to $V_{RL} = 0$ ($V_{RL} = 10$). In the case of vanishing over-dot tunneling channel (the left panel) the current has a simple structure – a single peak localized in the middle between μ_L and μ_R for smaller values of μ_L . The width of this peak increases with increasing $|\mu_L|$ ($\mu_R = 0$) and for greater values of $|\mu_L|$ the current is almost independent of ε_d localized inside the energy region between μ_R and μ_L . For non-vanishing over-dot tunneling (Fig. 4, the right panel) the curves $\langle j_L(t) \rangle$ become asymmetric. With increasing source-drain bias, the current possesses greater values in comparison with the $V_{RL} = 0$ case due to the direct tunneling between both leads. Note, however, that due to the interference effects the resulting $\langle j_L(t) \rangle$ curves are asymmetric. The interference effects are most visible approximately for ε_d lying in the region (μ_R, μ_L) .

In Fig. 5 we show the average current $\langle j_L(t) \rangle$ vs. the left lead chemical potential μ_L for several values of ε_d . For vanishing V_{RL} the corresponding curves are nearly asymmetric with the asymmetry point $\mu_L = \varepsilon_d$. With increasing μ_L at fixed ε_d the current achieves a constant value depending on the position of the QD energy level ε_d with respect to the $\mu_R = 0$. It means, that electrons which occupy the lead energy levels not too distant from ε_d take part in the tunneling process. For greater μ_L most of the lead energy levels lying far away from the ε_d are inactive in the tunneling between leads through the QD energy level. However, at non-vanishing V_{RL} (see the right panel of Fig. 5) these lead energy levels are active and the current $\langle j_L(t) \rangle$ vs. μ_L is of much richer structure. The current is nearly linearly growing with the increasing μ_L (for larger μ_L) because the tunneling through the QD can be neglected compared with the direct tunneling between both leads. The clearly visible interference effects appear only for μ_L not too distant from ε_d .

In Fig. 6 we show the derivatives of the average current vs. the QD energy level ε_d obtained for some values of μ_L . These are the results of the intersection of the surfaces

given in Fig. 2 with the planes at constant values of μ_L or the results of the differentiation of curves shown in Fig. 4. Again, the most visible differences between the results obtained for $V_{RL} = 0$ and $V_{RL} \neq 0$ are present for the QD energy level ε_d localized approximately between chemical potentials of both leads (compare, for example, the curves calculated for $\mu_L = 8$).

Fig. 7 presents the comparison of the $d\langle j_L(t) \rangle / d\mu_L$ vs. μ_L curves calculated for vanishing V_{RL} (left panels) and for $V_{RL} = 10$ (right panels) for two different values of the amplitudes Δ_L ($\Delta_d = \Delta_L/2$, $\Delta_R = 0$). At the vanishing value of V_{RL} , the shape of the curves is symmetrical in relation to the values $\mu_L = \varepsilon_d$ although for greater Δ_L some shoulders appear on both sides of the corresponding peaks in the distance $\sim \Delta_L/2$ from the curve centres. For non-vanishing V_{RL} , the corresponding curves are approximately asymmetric and for large μ_L they tend to constant, non-zero values corresponding to linear increasing of the current at large μ_L . It is interesting that with the increasing amplitudes Δ_L and Δ_d very clear structures appear on both sides of the corresponding curves. Note, that all these curves can be obtained, for example, from the one calculated for $\varepsilon_d = 0$ and moved along the μ_L -axis by the corresponding value (equal to ε_d).

Fig. 8 shows the dependence of the average current $\langle j_L(t) \rangle$ on the QD energy level ε_d and the direct coupling V_{RL} between both leads. The upper and bottom panels correspond to different values of the amplitude Δ_L ($\Delta_d = \Delta_L/2$). A very distinct transition from the symmetric to nearly antisymmetric behaviour of the current vs. ε_d curves is observed with the increasing value of the over-dot additional coupling between the leads for both values of Δ_L . The larger amplitudes of the left lead and QD levels oscillations result only in some broadening of the characteristic features of the average current vs. V_{RL} and ε_d surface and do not introduce any additional structures on these surfaces (for the range of parameters where $\omega \sim \Gamma$ and $\mu_L - \mu_R$ is not very small).

Fig. 9 presents the average current $\langle j_L(t) \rangle$ obtained for the case in which only the QD energy level ε_d oscillates with some frequency ($\omega > \Gamma$) and for the small source-drain voltage $\mu_L - \mu_R = 0.2$. The subsequent panels a, b, c and d correspond to the increasing value of the amplitude Δ_d and the different curves (broken, thin, thick and very thick) describe the QD without the over dot channel, $V_{RL} = 0$, and with this channel at $V_{RL} = 4, 7$ and 10 , respectively. For vanishing V_{RL} (broken curves) we observe for small amplitude Δ_d only a central resonant peak (Fig. 9a). With increasing Δ_d , the subsequent peaks appear and the distance between them and the central peak is an integer multiple

of the frequency ω (sidebands). The location of peaks is independent of the amplitude Δ_d but their relative intensity values change and with increasing Δ_d the height of the central peak is reduced. For the relatively large amplitude Δ_d , the heights of the two neighbouring peaks (at $\varepsilon_d \pm \omega$) are approximately equal to the height of the central peak. If we take the additional over-dot tunneling channel into consideration, especially for small Δ_d , the asymmetric shape of the current curve is observed and this asymmetry increases with the increasing strength of the over-dot coupling between both leads. With the increasing amplitude Δ_d this asymmetry is reduced largely due to the extra, photon-assisted tunneling peaks whose strength increases with the increasing Δ_d . For sufficiently large values of Δ_d and V_{RL} the functional dependence of the average current on the QD energy level ε_d is nearly the same for vanishing and non-vanishing over-dot tunneling channels. There is only one difference – for large V_{RL} the corresponding curve is shifted to the higher values due to the direct channel between both leads.

The last two Figures 10, 11 are devoted to the analysis of the average current $\langle j_L(t) \rangle$ dependence on the oscillation period $2\pi/\omega$ of the external fields. In Fig. 10 we show the overall dependence of $\langle j_L(t) \rangle$ on $2\pi/\omega$ and the QD energy level ε_d . The upper (lower) part of the Figure presents the results for the vanishing (non-vanishing) over dot channel between both leads. The most visible differences between averaged currents calculated for $V_{RL} = 0$ and $V_{RL} \neq 0$ can be observed for $\varepsilon_d \leq \mu_L$, especially for small values of $2\pi/\omega$. More detailed analysis of the $\langle j_L(t) \rangle$ dependence on the oscillation period $2\pi/\omega$ is shown for some chosen values of the parameters ε_d and V_{RL} in Fig. 11. The thin (thick) curves correspond to $\varepsilon_d = 5$ ($\varepsilon_d = 1$) and the solid (broken) curves correspond to $V_{RL} = 4$ ($V_{RL} = 0$). Additionally, we give the results for two values of the amplitude Δ_L ($\Delta_d = \Delta_L/2$, $\Delta_R = 0$), i.e. for $\Delta_L = 5$ and $\Delta_L = 10$, the left and the right parts of Fig. 11 respectively. We observe the characteristic average current oscillations damped with increasing $2\pi/\omega$ for ε_d lying in the central part between the left and right chemical potentials (see also [9]). These oscillations are present for both $V_{RL} = 0$ and $V_{RL} \neq 0$ and more visible for greater amplitudes Δ_L and Δ_d but the maxima and minima of the oscillating average current are localized at the same value of the oscillation period. Note, that the existence of the additional over-dot tunneling channel results approximately in shifting the corresponding curves to higher values without any additional serious modifications. For the QD energy level lying away from the middle point between the left and right chemical potentials, the average current is still an oscillating function of

$2\pi/\omega$ although these oscillations are less transparent and their oscillation period is much longer.

To conclude, we have provided a detailed investigation of a QD connected to two leads with an additional over-dot tunneling channel. The harmonic external microwave fields were considered as applied to the QD and two leads which result in time-dependence of the corresponding QD and leads energy levels. The QD charge and the average current flowing in this system were calculated within the evolution operator technique. The corresponding matrix elements of the evolution operator required for the calculation of the QD charge and current were presented in the form of the infinite series of multiple time integrals of the functions containing the information about the coupling between the QD and leads or in the form of the integro-differential equation. Applying the WBL approximation we were able to obtain all required evolution operator matrix elements in closed forms and give the final analytical expressions for the QD charge and current. We have performed the extended numerical calculations for the QD charge, the average current and the derivatives of the current with respect to the gate and source-drain voltages (Fig. 4). The most spectacular influence of the additional bridge tunneling channel is visible in the $\langle j_L(t) \rangle$ dependence vs. the position of the QD energy level at the constant source-drain voltage. Going from the vanishing values of the over-dot tunneling channel strength to the non-vanishing one due to the interference effects, the corresponding curve transforms from the symmetric to nearly antisymmetric shape. Similar influence of the non-vanishing V_{RL} is visible in the dependence of $d\langle j_L(t) \rangle/d\mu_L$ vs. μ_L (Fig. 7). The characteristic behaviour of the average current vs. the QD energy level position at the small source-drain voltage is observed for the case when the external oscillating field is applied only to the QD (Fig. 9). For the vanishing over-dot tunneling channel at the small amplitude Δ_d , the main resonant peak is only observed and with the increasing amplitude Δ_d the next peaks localized at ε_d equal to the multiplicity of ω appear corresponding to the photon-assisted tunneling. In that case the current is a symmetric curve centered around the main resonant peak. For the nonvanishing over-dot tunneling channel and small amplitudes Δ_d , the character of the dependence of the average current on the QD energy level position transforms with increasing V_{RL} from the symmetrical to nearly antisymmetrical behaviour. This tendency to the antisymmetrical behaviour with increasing V_{RL} at small amplitude Δ_d is reduced with increasing Δ_d . For sufficiently large amplitude Δ_d the overall behaviour of the average current vs. ε_d is very similar for different values

of V_{RL} and does not manifest the tendency for the antisymmetry with increasing V_{RL} .

Literature

1. T. H. Oosterkamp, L.P. Kouwenhoven, A.E.A. Koden, N.C. van der Vaart, C.J.P.M. Harmans, Phys. Rev. Lett. **78**, 1536 (1997)
2. Qing-feng Sun, Tsung-han Lin, Phys. Rev. **B56** 3591 (1997)
3. Qing-feng Sun, Jian Wang, Tsung-han Lin, Phys. Rev. **B58**, 13007 (1998)
4. C.A. Stafford, N.S. Wingreen, Phys. Rev. Lett. **76**, 1916 (1996)
5. Qing-feng Sun, Tsung-han Lin, J. Phys.: Condens. Matter **9**, 3043 (1997)
6. L.P. Kouwenhoven, A.T. Johnson, N.C. van der Vaart, A. van der Enden, C.J.P.M. Harmans, C.T. Foxon, Z. Phys. B, Condens. Matter **85**, 381 (1991)
7. H.-K. Zhao, J. Wang, Eur. Phys. J. **B9**, 513 (1999)
8. Y. Goldin, Y. Avishai, Phys. Rev. **B61**, 16750 (2000)
9. A.-P. Jauho, N.S. Wingreen, Y. Meir, Phys. Rev. **B50**, 5528 (1994)
10. Qing-feng Sun, Tsung-han Lin, J. Phys.: Condens. Matter **9**, 4875 (1998)
11. U. Fano, Phys. Rev. **124**, 1866 (1969)
12. J. Göres, D. Goldhaber-Gordon, S. Heemeyer, M.A. Kastner, H. Shtrikman, D. Mahalu, U. Meirav, Phys. Rev. **B62**, 2188 (2000)
13. M. Plihal, J.W. Gadzuk, Phys. Rev. **B63**, 085404 (2001)
14. V. Madhavan, W. Chen, T. Jamneala, M.F. Crommie, N.S. Wingreen, Science **280**, 567 (1998)
15. O. Ujsaghy, J. Kroha, L. Szunyogh, A. Zawadowski, Phys. Rev. Lett. **85**, 2557 (2000)

16. B.R. Bułka, P. Stefański, Phys. Rev. Lett. **86**, 5128 (2001)
17. M. Tsukada, N. Shima, in: “Dynamical Processes and Ordering on Solid Surfaces”,
Eds. A. Yoshimori and M. Tsukada (Springer, Berlin 1995), p. 34
18. T.B. Grimley, V.C.J. Bhasu, K.L. Sebastian, Surf. Sci. **121**,305 (1983)
19. T. Kwapiński, R. Taranko, Physica E, in press

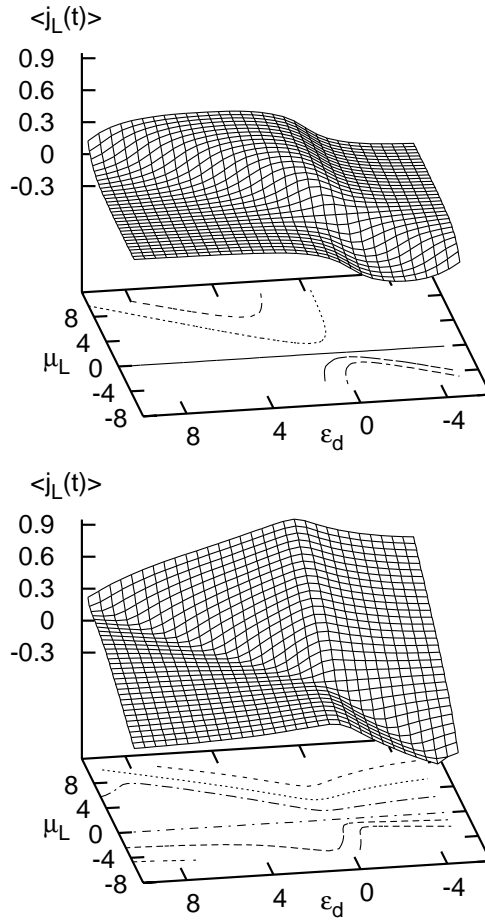


Figure 1: The average current $\langle j_L(t) \rangle$ against the left lead chemical potential μ_L and QD energy level ε_d for $V_{RL} = 0$ (the QD without the over-dot channel, the upper panel) and for $V_{RL} = 10$ (lower panel). $\mu_R = 0$, $V = 4$, $\Delta_L = 2$, $\Delta_d = 1$, $\Delta_R = 0$, $\omega = 2$ and all energies are given in Γ units.

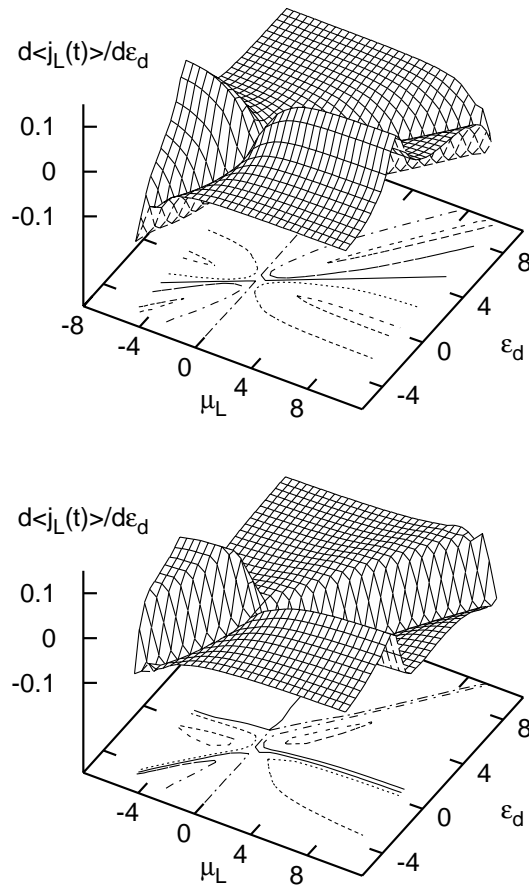


Figure 2: The derivatives of the average current with respect to the QD energy level ε_d , $d\langle j_L(t) \rangle / d\varepsilon_d$, against μ_L and ε_d for $V_{RL} = 0$ (upper panel) and for $V_{RL} = 10$ (lower panel). The other parameters as in Fig. 1.

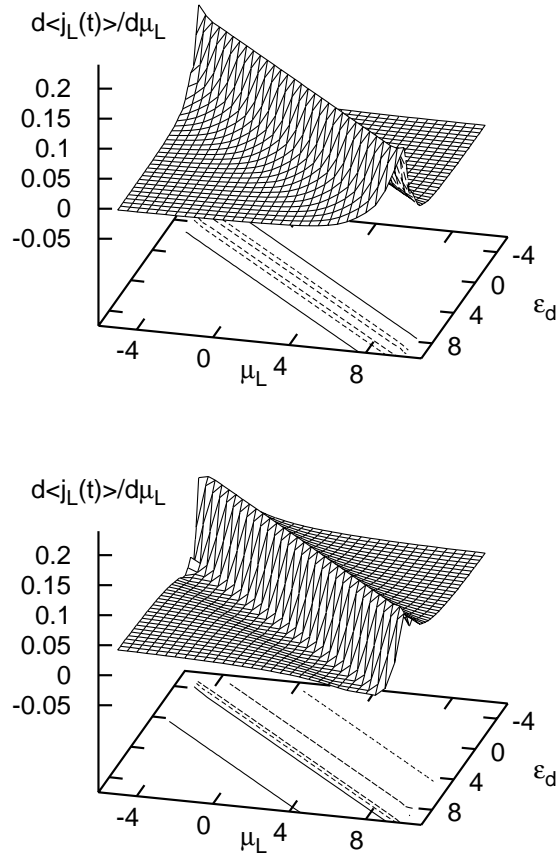


Figure 3: The derivatives of the average current $d\langle j_L(t) \rangle / d\mu_L$, against μ_L and ε_d for $V_{RL} = 0$ (upper panel) and for $V_{RL} = 10$ (lower panel). The other parameters as in Fig. 1.

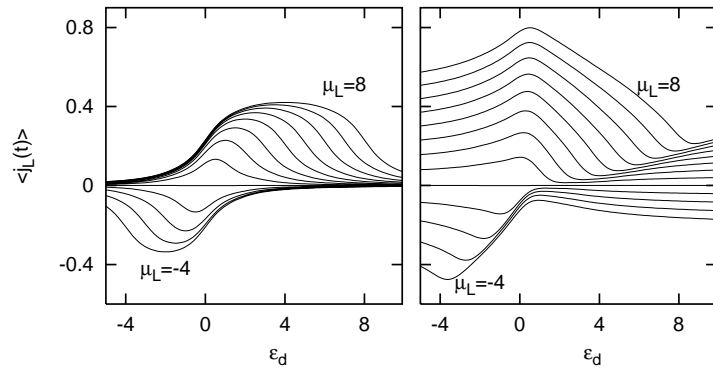


Figure 4: The average current $\langle j_L(t) \rangle$ against ε_d for given values of μ_L (beginning from $\mu_L = -4$ up to $\mu_L = 8$). The left and right panels correspond to $V_{RL} = 0$ and $V_{RL} = 10$, respectively, and the other parameters as in Fig. 1.

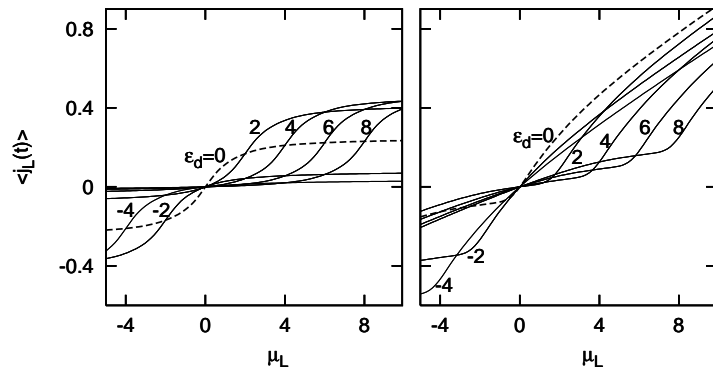


Figure 5: The average current $\langle j_L(t) \rangle$ against μ_L for given values ε_d (beginning from $\varepsilon_d = -4$ up to $\varepsilon_d = 8$). The broken curves correspond to $\varepsilon_d = 0$. The left (right) panel corresponds to $V_{RL} = 0$ ($V_{RL} = 10$). The other parameters as in Fig. 1.

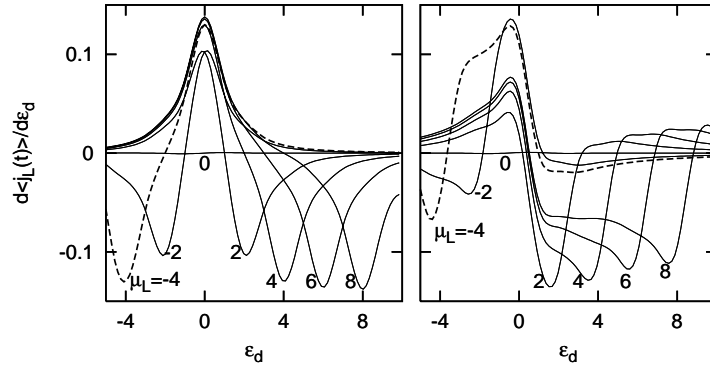


Figure 6: The derivatives of the average current $d\langle j_L(t) \rangle / d\varepsilon_d$ with respect to the QD energy level ε_d for given values of μ_L (beginning from $\mu_L = -4$ up to $\mu_L = 8$). The broken curves correspond to $\mu_L = -4$. The left (right) panel corresponds to $V_{RL} = 0$ ($V_{RL} = 10$) and the other parameters as in Fig. 1.

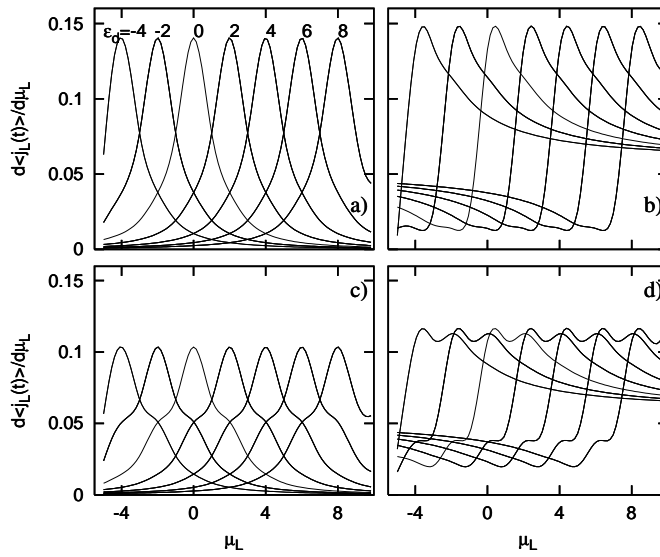


Figure 7: The derivatives of the average current with respect to μ_L , $d\langle j_L(t)\rangle/d\mu_L$, for given values of ε_d (beginning from $\varepsilon_d = -4$ up to $\varepsilon_d = 8$). The left (right) panels correspond to $V_{RL} = 0$ ($V_{RL} = 10$) and upper (lower) panels correspond to $\Delta_L = 2$ ($\Delta_L = 4$). The other parameters as in Fig. 1.

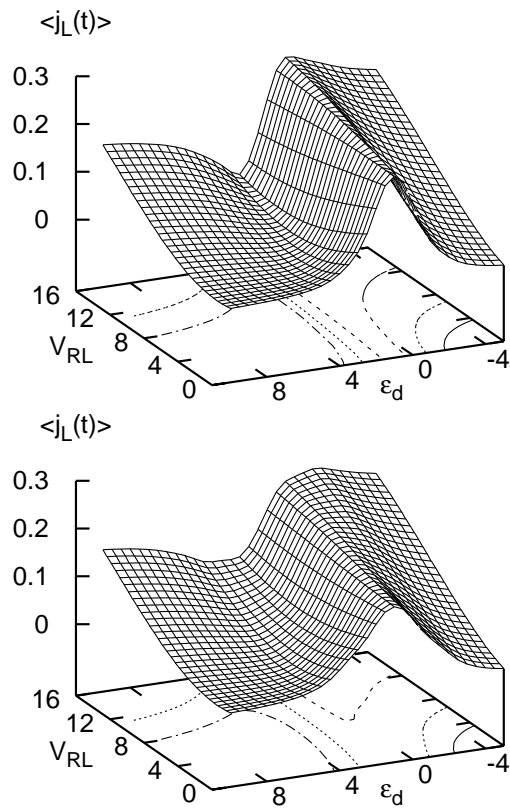


Figure 8: The average current $\langle j_L(t) \rangle$ against V_{RL} and ε_d . The upper (lower) panel corresponds to $\Delta_L = 2$, $\Delta_d = 1$ ($\Delta_L = 4$, $\Delta_d = 2$). $\mu_L = 2$, $V = 4$.

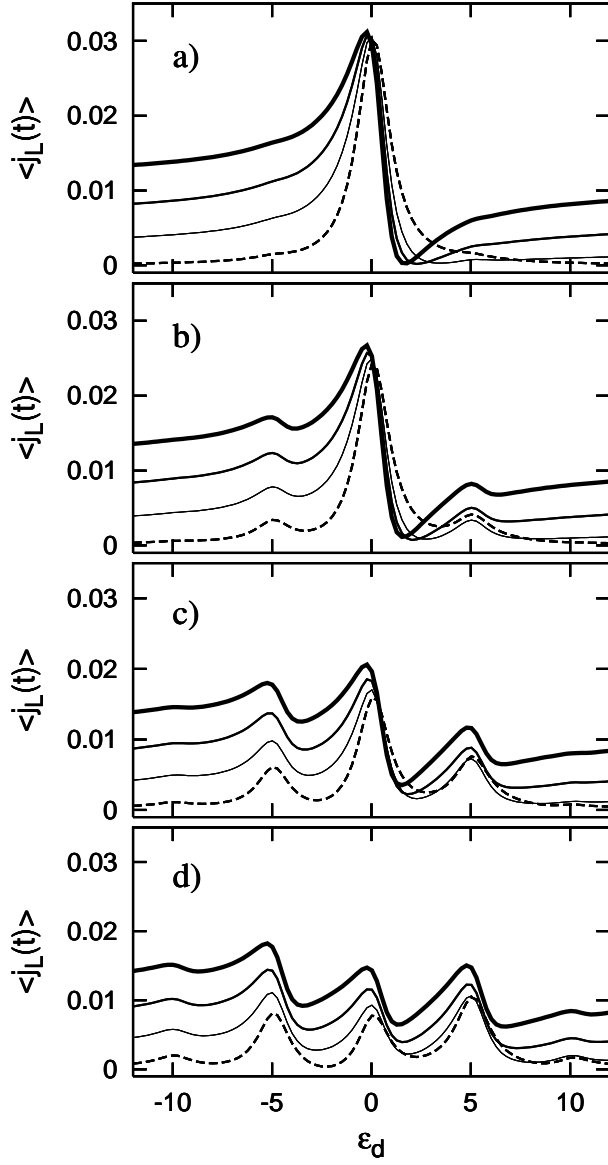


Figure 9: The average current $\langle j_L(t) \rangle$ against ε_d for the oscillating QD energy level at $V_{RL} = 0, 4, 7, 10$ – broken, thin, thick and very thick curves, respectively. The panels a, b, c and d correspond to $\Delta_d = 1, 3, 5$ and 7 , respectively. $\omega = 5$, $\Gamma = 1$, $V = 4$, $\mu_L = 0.2$, $\Delta_L = \Delta_R = 0$.

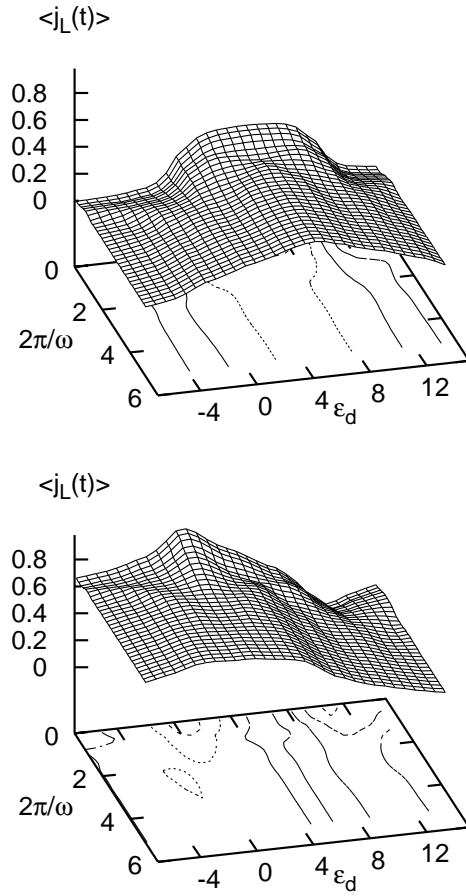


Figure 10: The average current $\langle j_L(t) \rangle$ against ε_d and the period of the time oscillation of the external field for $V_{RL} = 0$ – the upper panel and for $V_{RL} = 10$ – the lower panel. $V = 4$, $\mu_L = 10$, $\Delta_L = 10$, $\Delta_d = 5$, $\Delta_R = 0$.

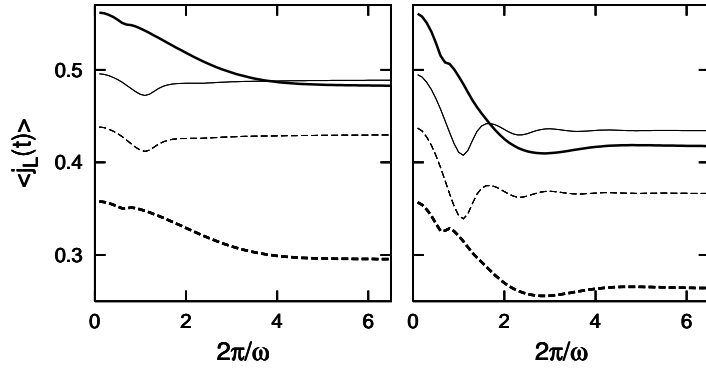


Figure 11: The average current $\langle j_L(t) \rangle$ against the period of the time oscillation of the external field for $V_{RL} = 0$ – the broken curves, and for $V_{RL} = 4$ – the solid curves. The thin (thick) curves correspond to $\varepsilon_d = 1$ ($\varepsilon_d = 5$). The left (right) panel corresponds to $\Delta_L = 5, \Delta_d = 2.5$ ($\Delta_L = 10, \Delta_d = 5$). $\Delta_R = 0, V = 4, \mu_L = 10$.